Supplemental Document

Optics Letters

Full-field measurement of complex objects illuminated by an ultrashort pulse laser using delay-line sweeping off-axis interferometry: supplement

WENHUI YU, XIANG LI, RUI HU, JUNLE QU, AND LIWEI LIU*

College of Physics and Optoelectronic Engineering, Shenzhen University, Shenzhen 518000, China
**Corresponding author: liulw@szu.edu.cn*

Supplement DOI: https://doi.org/10.6084/m9.figshare.14611722

Parent Article DOI: https://doi.org/10.1364/OL.421313

1. Simulation on the interferogram generation

The complex field distribution of a femtosecond laser with Gaussian intensity profile as well as Gaussian pulse shape can be expressed as:

$$E_S(x,y;t) = E_{S0}\exp\left(\frac{x^2+y^2}{2\sigma^2}\right)\exp\left(-\frac{t^2}{\tau_0^2}\right)\exp(i\omega_c t + i\varphi(x,y)), \quad \text{(S1)}$$

where σ is the spot width of the laser beam, τ_0 is the pulse duration, ω_c is angular frequency of the carrier wave and $\varphi(x,y)$ is the spatially-varying object phase distribution. The reference beam having an intersection angle of θ with the sample beam can be written as:

$$E_R(x,y;t) = E_{R0}\exp\left(\frac{x^2+y^2}{2\sigma^2}\right)\exp\left\{-\frac{[t-\tau(x,y)]^2}{\tau_0^2}\right\}\exp\{i\omega_c[t-\tau(x,y)]\}, \quad \text{(S2)}$$

where the position-dependent pulse delay $\tau(x,y) = [(x+y)\theta]/c$, with c as the speed of light. What is distinct to the interference of CW laser, as can be seen from Eq. (S2), is that the delay between the two beams not only introduces a phase shift (the last term in Eq. (S2)), which is responsible for the generation of fringes, but also introduces a mismatch between the two pulses envelope (the third term in Eq. (S2) and see Fig. 2(d) in the main text), which decreases the fringe visibility.

In the simulation for generating the interferogram shown in Fig. 2(a)-(c) in the main text, the sample phase was set $\varphi(x,y) = 0$, and the reference delay $\tau(x,y) = [(x+y)\theta]/c$. The carrier frequency was set as $\omega_c = 2\pi c/\lambda_c$ with $\lambda_c = 800\,nm$. The beam width σ was set to be 5 *mm*. At each time instant, the squared amplitude of the superposed complex field E_S+E_R was calculated, and was integrated over time, producing interferograms. The simulation results are shown in Fig. 2(a)-(c) in the main text for 20 *fs* and 100 *fs* pulse widths and intersection angles of 3 *mrad* and 60 *mrad*.

2. Complex field generation using phase-only SLM

Four adjacent pixels along y-axis formed a superpixel that can generate any complex field at the first order diffraction spot. As shown in Fig. S1(a), the optical path differences at the first order diffraction spot between the forming pixels are 0, π/2, π and 2π/3. Having this, the real (imaginary) parts of a complex field $E(x,y) = E_r(x,y) + iE_i(x,y)$ can be controlled by combination of pixel 1 and pixel 3 (pixel 2 and pixel 4 for imaginary part).

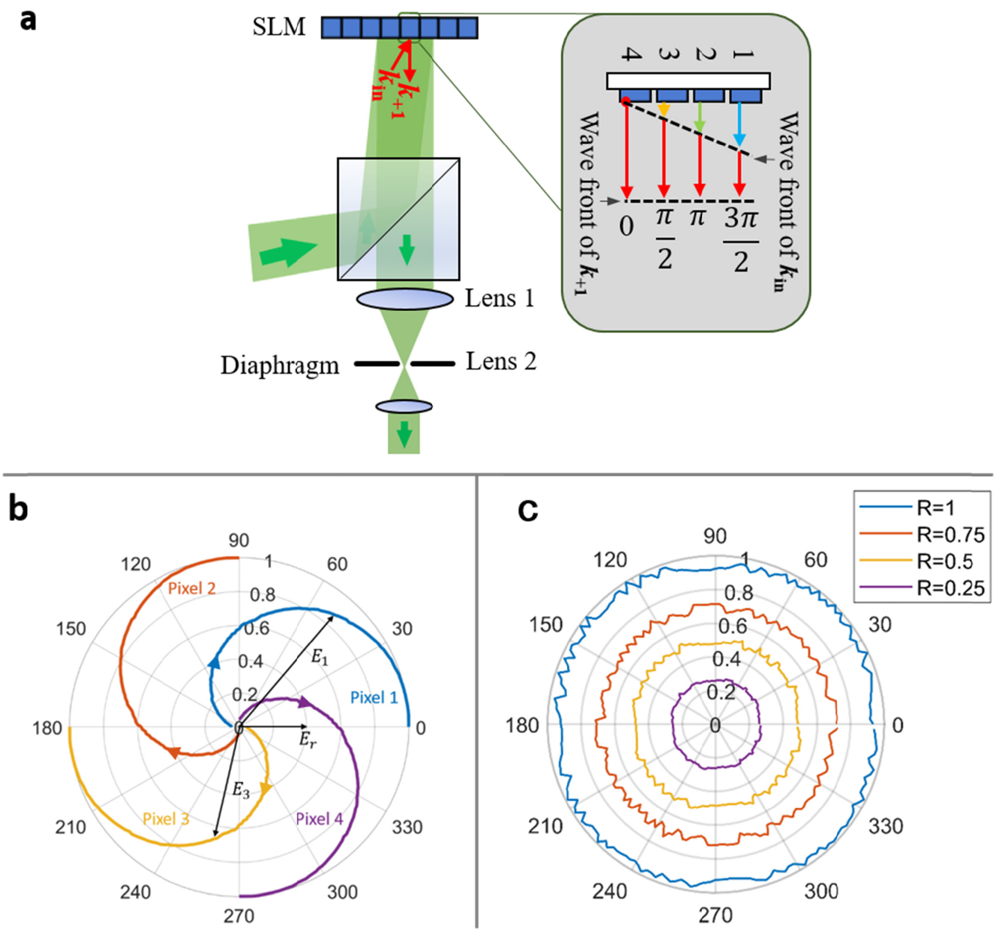

Fig. S1. Arbitrary complex field generation using SLM. (a) Illustration of 4-pixel binning of a SLM. (b) Response curve of four binning pixels at the first diffraction spot. (c) Illustration of amplitude and phase decoupling using the 4-pixel binning method.

The voltages loaded to pixel 1 and pixel 3 should conform the following relationship:

$$\begin{cases} E_r = E_{1r} - E_{3r}, \\ E_1 = E_{1r} + i\phi, \\ E_3 = E_{3r} + i\phi, \end{cases} \tag{S11}$$

where $E_{1\mathrm{r}}$ and $E_{3\mathrm{r}}$ are the real parts of the fields modulated by pixel 1 and pixel 3, and ϕ is the imaginary part of the modulated fields. The destruction between pixel 1 and pixel 3 is resulted from the fact that they are π out of phase. Similarly, the voltages loaded to pixel 2 and pixel 4 should conform the following relationship:

$$\begin{cases} E_i = E_{2r} - E_{4r}, \\ E_2 = E_{2r} + i\psi, \\ E_4 = E_{4r} + i\psi, \end{cases} \tag{S12}$$

where $E_{2\mathrm{r}}$ and $E_{4\mathrm{r}}$ are the real parts of the fields modulated by pixel 2 and pixel 4, and ψ is the imaginary part of the modulated fields. Since there is $\pi/2$ phase difference between pixel 1 and pixel 2, as well as between pixel 3 and pixel 4, the E_r in Eq. (S11) and the E_i in Eq. (S12) form the real and imaginary parts of the desired complex field, respectively. In the experiment, the amplitude and phase pattern were combined to form a desired complex field. The real and imaginary parts of the complex field were then calculated in order to determine the voltages loaded to each subpixel. To find the relationship between the applied voltage and the modulation curve of the SLM, we used diffraction technique and placed a binary grating with duty cycle of 50% on the SLM, which is equivalent to the technology described in Ref. 22. The amplitude response at the first order diffraction spot for each pixel was measured as shown by the polar plot in Fig.S1 (b). The arrows denote the modulation value change direction when voltage increases. For accurately calibrated voltage-phase response curve (commonly called gamma curve), the amplitude changes from zero to maximum when the phase modulation changes from 0 to π. We have also tested the mutual interaction between the phase and amplitude as shown in Fig. S1 (c). It shows that the amplitude and phase are well decoupled, thus ensures us to generate complex objects without mutual interference between them.

Fig. S2 shows an example of complex field generation using 4-pixle binning, in which the amplitude is the image of the emblem of Shenzhen University (Fig.S2 (a)) and the phase is a standard test image of pepper (Fig.S2 (b)). The first order diffraction beam was imaged to the sample plane of the objective with an amplification of 1/12.5 and imaged by the objective. The detected image in Fig. S2(c) shows that the image of the emblem can be clearly seen on the camera. The phase pattern can also be recognized from the shape change of the interference fringe, shown in Fig.S2 (d) once the delay line was adjusted to a specific location.

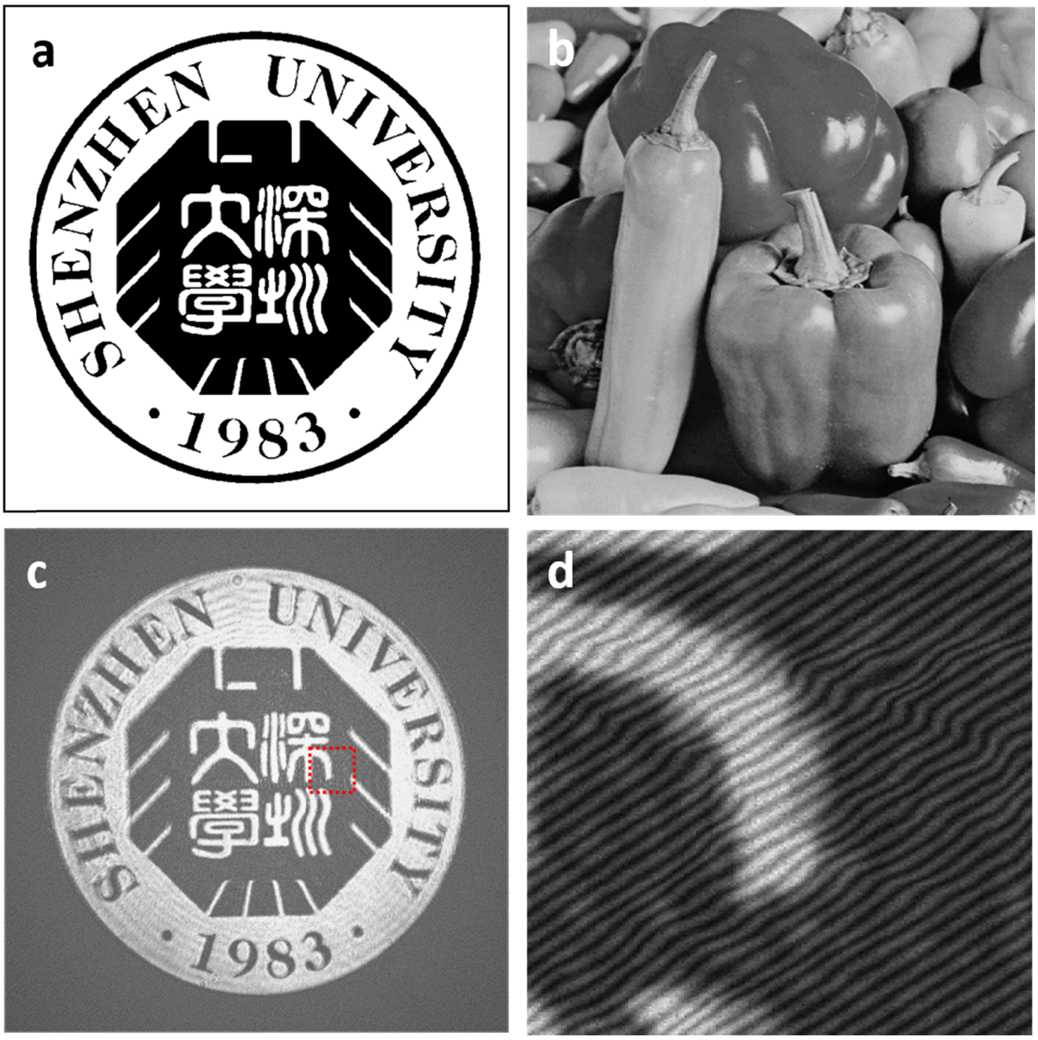

Fig. S2. Complex pattern generated by SLM using four-pixel binning. (a) and (b) are the amplitude and phase pattern loaded to the SLM, respectively. (c) is the generated image interfered with the reference beam, i.e., the interferogram. (d) is the zoom-in view of the area highlighted in the red dashed box in (c). The phase pattern highlighted in the red dashed box in (c) can be well-recognized from the changes of the fringe direction in (d).

For the 72-sector star target, a 468x468 gray scale image, containing 72 sectors of phase from 0-2π was firstly generated by Matlab, as shown in Fig. S3. Then, the complex field, which the amplitude was the emblem of Shenzhen University and the phase was the 72-sector star target, was generated by the SLM using the method described above. Since the pixel size of the SLM is 9.2 µm, the image size on the object plane of the objective was about L=9.2*468/12.5= 344 µm.

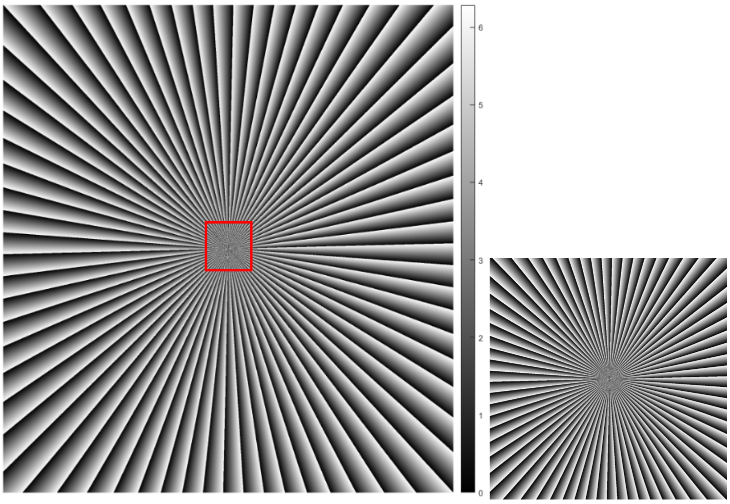

*Fig. S3. The phase pattern of a 72-sector star target applied to the SLM for the resolution test in Fig. 4 of the main text. (a) the 468*x*468 gray scale image. (b) the zoom-in view of the pattern in the red box of (a).*

The highest frequency in the center of Fig.4 (b) and (d) was ultimately limited by the pixel size of both the SLM generating the star target (a_s=9.2 μm) and the imaging objective (a_o=6.5 μm) by:

$$f_{\max} = \min\left\{\frac{M_1}{a_s}, \frac{M_2}{a_o}\right\} = \min\left\{\frac{12.5}{9.2 \times 10^{-3}}, \frac{40}{6.5 \times 10^{-3}}\right\} mm^{-1} = 1358\, mm^{-1}$$

where M_1=12.5 and M_2=40 are the shrinking and amplification factors of the shrink lens and the objective, respectively.

The lowest frequency at the corners is:

$$f_{\min} = \frac{72}{2\pi\frac{\sqrt{2}}{2}L} = 47.1\, mm^{-1}.$$

where L=344 μm is the image size of the star target on the object plane.